

Original Article

Antitumor effect of *Escherichia coli*-derived outer membrane vesicles on neuroblastoma *in vitro* and *in vivo*

Liming Jin^{1,2,3,†}, Zhaoxia Zhang^{1,2,3,†}, Xiaojun Tan^{1,2,3}, Zhaoying Wang^{1,2,3}, Bo Tang^{1,2,3}, Zhang Wang^{1,2,3}, Mujie Li^{1,2,3}, Tao Mi^{1,2,3}, Lianju Shen^{2,3}, Chunlan Long^{2,3}, Guanghui Wei^{1,2,3}, and Dawei He^{1,2,3,*}

¹Department of Urology, Children's Hospital of Chongqing Medical University, Chongqing 400014, China, ²Chongqing Key Laboratory of Children Urogenital Development and Tissue Engineering, Chongqing 400014, China, and ³China International Science and Technology Cooperation base of Child development and Critical Disorders; National Clinical Research Center for Child Health and Disorders; Ministry of Education Key Laboratory of Child Development and Disorders; Chongqing Key Laboratory of Pediatrics; Children's Hospital of Chongqing Medical University, Chongqing 400014, China

[†]These authors contributed equally to this work.

*Correspondence address. Tel: +86-23-63326521; E-mail: hedawei@hospital.cqmu.edu.cn

Received 1 November 2021 Accepted 2 March 2022

Abstract

Bacterial outer membrane vesicles (OMVs) are spherical microbubbles that contain biological content and are produced by gram-negative bacteria. The use of OMVs as adjuvants for cancer immunotherapy or as drug carriers for targeted therapies has attracted the interest of many scholars. However, it is unclear whether OMVs can exert direct antitumor effects and whether OMVs can inhibit pediatric tumors. Here, we explore the potential of *Escherichia coli*-derived OMVs to directly suppress neuroblastoma. Our results demonstrate the antitumor effects of OMVs *in vitro* and *in vivo*, and no serious adverse reactions were observed. OMV uptake into the cytoplasm and nucleus directly decreases cell stemness, DNA damage, apoptosis and cell cycle arrest, which may be the mechanisms by which OMVs suppress tumors. Our results demonstrate the potential of bacterial OMVs to be used as antitumor adjuvant therapies, increasing the number of candidates for the development of cancer therapies in the future. More relevant studies are urgently needed to demonstrate the efficacy and safety of OMVs.

Key words outer membrane vesicles, neuroblastoma, P53, apoptosis

Introduction

Cancer is the greatest health problem that threatens humankind, as tens of millions of people die from cancer each year [1]. The identification of newer and more effective treatments is one of the most significant missions of scholars in the medical field. Today, a large number of studies have shown that changes in the gut microbiome are intricately linked to the development of cancers [2]. Some species of intestinal flora and their biological products have been used in cancer therapy, especially in immunotherapy, and have shown surprising results [3,4]. Outer membrane vesicles (OMVs) are vesicle-like substances that resemble cellular exosomes and contain a variety of bioactive substances, including proteins, lipids, nucleic acids and metabolites. OMVs have been found to be safe and efficient in tumor therapy. The discovery of bacterial OMVs

has provided a new platform for the use of bacteria in cancer therapy [5–7].

Currently, the exploration of bacterial OMVs focused more on their use as either adjuvants for immunotherapy or drug carriers for targeted therapies [8,9]. Kim *et al.* [10] reported that *Escherichia coli*-derived OMVs (*E. coli*-OMVs) exert unique antitumor effects in mice with colon cancer via IFN- γ . OMVs derived from *Salmonella typhimurium* have significant abilities to kill human colon, breast and hepatocellular carcinoma cells [11]. However, current studies on the antitumor effect of OMVs focused mostly on adult cancers, and little attention has been paid to their effects on pediatric tumors. It is interesting to explore whether bacterial OMVs can exert antitumor effects on pediatric tumors independently.

Neuroblastoma (NB) is one of the most common extracranial

solid tumors diagnosed in early childhood, accounting for 7% of all solid tumors in children [12]. Due to the biological characteristics of NB and its clinical presentation including its early onset, some children have metastatic lesions at the first diagnosis. A significant proportion of high-risk patients have a low survival rate even after undergoing comprehensive therapy with traditional surgery, chemotherapy, radiotherapy and other therapies [13,14]. Therefore, new approaches for the treatment of NB are urgently needed.

In this study, we explored the antitumor effects of OMVs derived from *E. coli* on human NB cells *in vitro* and performed a preliminary exploration of possible inhibitory mechanisms. We established a human NB subcutaneous xenograft tumor model in nude mice and explored whether *E. coli*-OMVs could exert antitumor effects *in vivo*. Further exploration of the antitumor activity of bacterial OMVs will benefit countless cancer patients, and we believe it will contribute to the broader picture of cancer treatment.

Material and Methods

Bacterial strain and *E. coli*-derived OMV preparation

Escherichia coli strain ATCC 11775 was obtained from the Laboratory Clinical Department of the Children's Hospital of Chongqing Medical University who purchased the strain from American Type Culture Collection (ATCC, Manassas, USA). *E. coli* was cultured in LB liquid growth medium (GA15KA7279; Sangon Biotech, Shanghai, China) at 37°C with shaking (180 rpm). Once the absorbance of an *E. coli* culture suspension reached 1.0, the suspension was centrifuged at 6000 *g* for 20 min at 4°C, and then, the supernatant was filtered through sterile membrane filters (0.45- μ m pore size; Millipore, Billerica, USA) twice to remove bacterial sediments. *E. coli*-derived OMVs were obtained from the filtrate by ultrafiltration (2500g/min, 10 min, 4°C) using 100-kDa Centrifugal Filter Unit (UFC910096; Millipore), followed by ultracentrifugation (110,000 *g*, 70 min, 4°C) with the Optima L-80xp ultracentrifuge (Beckman, Pasadena, USA). The precipitate containing the OMVs was collected and dissolved in phosphate-buffered saline (PBS). The purified OMVs were filtered through a 0.45- μ m pore size filter. The protein concentration was measured using a BCA protein assay kit (P0012; Beyotime, Shanghai, China). The sample was aliquoted and stored at -80°C until use.

Characterization of *E. coli*-OMVs

The size and shape of *E. coli*-OMVs were evaluated with an S-3000N transmission electron microscope (Hitachi, Tokyo, Japan). The size distribution was evaluated with nanoparticle tracking analysis (NTA), which was performed at VivaCellBiosciences (Shanghai China) with ZetaView PMX 110 (Particle Metrix, Meerbusch, Germany) and the corresponding software ZetaView 8.04.02. A bacterial lipopolysaccharide (LPS) ELISA kit (Fengbin Technology, Wuhan, China) was used to quantify the LPS levels in the extracted *E. coli*-OMVs following the manufacturer's instructions.

Cell culture

The human neuroblastoma cell line SK-N-SH was purchased from ATCC and preserved in our laboratory. The HEK293 cell line and human neuroblastoma cell line SH-SY5Y were purchased from Procell Life Science & Technology (Wuhan, China) and preserved in our laboratory. SK-N-SH cells were cultured in Dulbecco's modified Eagle's medium (DMEM) nutrient mixture F-12 (DMEM/F12) (Gibco, Carlsbad, USA) supplemented with 10% fetal bovine serum

(2045686 CP FBS; Gibco) at 37°C in 5% CO₂. HEK293 cells and SH-SY5Y cells were cultured in DMEM supplemented with 10% fetal bovine serum at 37°C in 5% CO₂.

E. coli-OMV internalization assay

E. coli-OMVs were incubated with the fluorescent lipophilic tracer PKH26 (PKH26 Red Fluorescent Cell Linker Kit; Sigma-Aldrich, St Louis, USA). PKH26-labelled *E. coli*-OMVs were incubated with SK-N-SH cells for 6 and 12 h. After incubation, the cells were fixed with 4% paraformaldehyde. DAPI was added to label the nuclei and incubated for 60 min in the dark at room temperature. Then, the samples were examined using a C2 Plus confocal microscope (Tokyo, Japan).

Cell proliferation and IC₅₀ assay

Cell proliferation was examined by CCK-8 assay using a Cell Counting Kit-8 (HY-K0301; MedChemExpress, Shanghai, China). Briefly, different concentrations of *E. coli*-OMVs were added to the cells, and the optical density (OD) was measured to calculate the cell viability and the half maximal inhibitory concentration (IC₅₀) of *E. coli*-OMVs. SK-N-SH, SH-SY5Y and HEK293 cells were cultured for 12 h. Then, the culture medium was replaced by complete medium supplemented with or without *E. coli*-derived OMVs at concentrations of 2, 4, 8, 16, 32, 64, 128, 256, and 512 μ g/mL (1.8 \times 10⁸ particles/ μ g), and the cultures were incubated for 48 h. At the indicated time points, CCK-8 reagent was added and incubated with the cells for 2 h at 37°C. Finally, the optical density (OD) was measured at 450 nm with a microplate reader (Bio-Rad, Hercules, USA). Cell viability was calculated as follows: Cell viability (%) = OD_{treated}/OD_{control} \times 100%. The half maximal inhibitory concentration (IC₅₀) of *E. coli*-derived OMVs was determined based on dose-response curves. In all, the dose of 3.15 \times 10¹⁰ particles/mL (IC₅₀) of *E. coli*-derived OMVs was chosen to repeat the assay described above at the indicated time points (0, 24, 48, 72 h) three times.

Cell cycle analysis

The cell cycle was examined using propidium iodide (PI)/RNase Staining Buffer Solution (550825; BD Pharmingen, Franklin Lakes, USA) and a flow cytometer (BD Biosciences, San Jose, USA) according to the manufacturer's protocols. Briefly, SK-N-SH cells were cultured with or without *E. coli*-OMVs (IC₅₀) for 48 h, and then the samples were incubated with PI/RNase staining buffer solution. Finally, the fluorescence intensities of the cells were measured on the flow cytometer and analysed with ModFit LT (version 3.2).

Cell apoptosis analysis

Apoptotic cell death was measured using a FITC Annexin V Apoptosis Detection Kit I (556547; BD Pharmingen) and One Step TUNEL Apoptosis Assay Kit (C1090; Beyotime) according to the manufacturer's protocols. Briefly, SK-N-SH and SH-SY5Y cells were treated with *E. coli*-OMVs (IC₅₀) for 48 h, and HEK 293 cells were treated with *E. coli*-OMVs (IC₅₀ of SK-N-SH) for 48 h. Then, all the cells were stained with Annexin V. SK-N-SH cells were treated with *E. coli*-OMVs (IC₅₀) for 48 h and then stained with TUNEL. SK-N-SH, SH-SY5Y and HEK293 cells were cultured for 12 h and subsequently incubated with or without *E. coli*-derived OMVs for 48 h. After the cells were trypsinized and washed with PBS, they were resuspended in binding buffer and treated with Annexin V-fluorescein isothiocyanate (FITC) and PI. The mixture was incubated for 15 min at

room temperature in the dark, and then the cells were analysed with the flow cytometer. The apoptosis rate was analysed using FlowJo software (version 10). In the TUNEL assay, *E. coli*-derived OMVs were incubated with SK-N-SH cells plated on circular cell slides for 48 h. Then, the samples were washed, fixed and covered and incubated with 0.3% Triton X-100 in PBS for 30 min at room temperature. Then, the samples were treated with TdT detection reagent for 60 min at room temperature in the dark. After extensive wash, the samples were incubated with DAPI for 60 min in the dark. Then, the samples were examined using the C2 Plus confocal microscope.

Migration and invasion assay

The migration capacity of cells was assessed by wound healing and Transwell assays. A scratch was made through monolayers of fully confluent SK-N-SH cells to create wounds. The culture medium was replaced by serum-free medium supplemented with or without *E. coli*-OMVs (IC₅₀). At 0, 24 and 48 h after scratching, the wound area was observed under an ECLIPSE Ti microscope (Nikon). Cell invasion was examined with 24-well Transwell chambers (353097; FALCON, San Diego, USA) coated with Matrigel. Cells in serum-free medium supplemented or without *E. coli*-OMVs (IC₅₀) were seeded into the upper chambers, and medium supplemented with 10% FBS with or without *E. coli*-OMVs (IC₅₀) was added into the lower chamber. After 24 and 48 h, the invaded wells were fixed in methanol and stained with crystal violet. The numbers of invaded cells were counted under the ECLIPSE Ti microscope after image acquisition. All the picture data were analysed with ImageJ software (version 1.53j).

Western blot analysis

Cells and tissues were lysed in RIPA buffer (P0013C; Beyotime) supplemented with 0.1mM phenylmethanesulfonyl fluoride (329-98-6; MedChemExpress). The lysed cells and tissues were centrifuged. A mitochondrial/cytoplasmic protein isolation kit (Sangon) was used to separately extract mitochondrial proteins and cytoplasmic proteins following the manufacturer's instructions. Equal amounts of proteins were subjected to 6%–12.5% SDS-PAGE (EpiZyme, Shanghai, China) and then transferred to polyvinylidene fluoride membranes (Millipore). The membranes were blocked with 5% fat-free milk. Immunoblotting was performed with antibodies targeting the following proteins: CD24, NANOG and OCT-3/4 (1:400; sc-19585, sc-374103 and sc-5279; Santa Cruz Biotechnology, Santa Cruz, USA); SOX-2 and MMP-9 (1:1000; EPR3131-ab92494 and EP1254-ab76003; Abcam, Cambridge, UK); BAX, BCL-2 and cleaved caspase-3, Cyt c, P21 and APAF (1:1000; #2772, #15071, #9661, #11940, #2947, and #8723); Cell Signaling Technology, Beverly, USA); MMP-2, PCNA, N-myc, GAPDH and VDAC1 (1:1000; 380817, 200947-2E1, 861964, R24404 and 380506; ZENBIO, Shanghai, China); VEGF (1:500; 19003-1-AP; Proteintech, Chicago, USA); and CDK2, cyclin A, phospho-P53, and P53 (1:500; WL01543, WL01841, WL02504 and WL01919; Wanleibio, Shanghai, China). The secondary antibodies were obtained from ZSGB-Bio (Shanghai, China). The enhanced chemiluminescence substrate (34075; Thermo Scientific, Waltham, USA) was used to visualize the protein bands. Images were captured with a ChemiDoc MP Imaging System (Bio-Rad), and densitometry analysis was carried out using Image Lab software (Version 3.0). The western blot images shown are representative of three independent repeats.

Therapeutic efficacy *in vivo*

BALB/c nude mice were purchased from SPF Biotechnology (Beijing, China) and housed under specific pathogen-free conditions. BALB/c mice were purchased from the Animal Experiment Center of Chongqing Medical University and housed under specific pathogen-free conditions. The study was performed according to international, national and institutional guidelines regarding the ethical treatment of animals, and the protocol was approved by the Ethics Committee of Chongqing Medical University. A total of 2×10^6 SK-N-SH cells suspended in 200 μ L of medium were subcutaneously injected into the right axilla of 4-week-old mice. After the tumor volume reached 90–100 mm³, the mice were randomized into five groups ($n=6$ per group) according to the tumor size. The mice were treated intravenously every 2 days with 250, 500, or 1000 μ g/mL *E. coli*-OMVs (0.15 mL per mouse) for a total of 8 days (four injections). The control groups were administered either PBS alone or nothing. The tumors were measured once a day with Vernier callipers, and the tumor volumes were calculated with the formula: $(\text{length} \times \text{width}^2)/2$. At the end point, the mice were sacrificed by cervical dislocation, and the subcutaneous tumors and other tissues were immediately harvested. Half of the tissues from each tumor were frozen in liquid nitrogen and stored at -80°C, and the other halves were fixed in 4% paraformaldehyde (PFA) for histopathological analysis. Blood was collected from the orbit, and the serum was separated and stored at -80°C. The serum was sent to the Laboratory Department of Children's Hospital of Chongqing Medical University for liver and kidney function tests, including ALT, AST, Cr and BUN measurements.

BALB/c mice (5 mice per group) were used to investigate whether OMVs induce a systemic inflammatory response. The mice were given tail vein injections of 1000 μ g/mL OMVs (containing 0.07 EU/L LPS) or 1000 μ g/mL standard LPS solution (containing 1.04 EU/L LPS) in 0.15 mL. The mice in each group were observed for 24 h, and anal temperature, mental status, hair color, urine and stool, activity and death were monitored. Blood was collected from the orbits; a 100- μ L sample was used to count and sort leukocytes, and the rest of the blood was used to measure blood glucose levels.

E. coli-OMVs were labelled with DIR fluorescent dye (20757ES25; Yeasen Biotechnology, Shanghai, China) according to the manufacturer's protocol. DIR-fluorescently labelled *E. coli*-OMVs were injected into tumor-bearing mice via the tail vein, and the animals were subject to *in vivo* imaging at 24 and 48 h. Then, the tumors and other organs were harvested for fluorescence quantification under a NightOWL II LB 983 In-vivo Imaging System (Berthold, Bad Wildbad, Germany) to observe the distribution of OMVs. Images were obtained by indiGO software (version 2.0.5.0).

Histopathological evaluation

For hematoxylin and eosin (HE) staining, tumors fixed with 4% PFA were embedded in paraffin. The samples were sliced into 4- μ m-thick sections and then deparaffinized and rehydrated. The slides were treated with hematoxylin, eosin, a graded series of alcohol, and xylene. All images were observed and captured under an ECLIPSE Ci microscope (Nikon). For the immunohistochemical staining of PCNA, MMP-9, and VEGF, sections were deparaffinized and subjected to heat-induced epitope retrieval in citrate solution. Then, the samples were treated with 3% hydrogen peroxide to block endogenous peroxidase activity and blocked with 0.5%

bovine albumin (A8020; Solarbio, Beijing, China). Anti-PCNA, MMP-9 and VEGF antibodies (as mentioned previously) were incubated with the sections for 12 h at 4°C, followed by incubation with an HRP-conjugated secondary antibody. The reaction product was detected by using a DAB Horseradish Peroxidase Color Development Kit (P0202; Beyotime), and the nuclei were stained with hematoxylin. All the samples were observed under the ECLIPSE Ci microscope, and images were captured.

TUNEL assay

The sample slides were deparaffinized and rehydrated as described for immunohistochemical analysis. Then, the samples were treated with proteinase K (20 µg/mL) and incubated with TdT detection reagent. Next, the samples were incubated with DAPI. All images were viewed and captured with an ECLIPSE 90i fluorescence microscope (Nikon).

Statistical analysis

Data are presented as the mean ± standard deviation (SD) as calculated with GraphPad Prism software (version 10). Statistical difference between two groups was determined using Student's *t*-test, and differences among more than two groups were determined using one-way ANOVA. A *P* value less than 0.05 was considered statistically significant.

Results

Characterization of *E. coli*-OMVs

Transmission electron microscopy (TEM) showed that *E. coli*-OMVs were nanospherical particles with different diameters in the nanometer range (Figure 1A). NTA examination showed that the diameter distribution of the nanospheres ranged from 45 to 280 nm, and the median size was 119.5 ± 2.95 nm (Figure 1B). The concentration of *E. coli*-OMVs was 1.83 × 10⁸ particles/µL in a

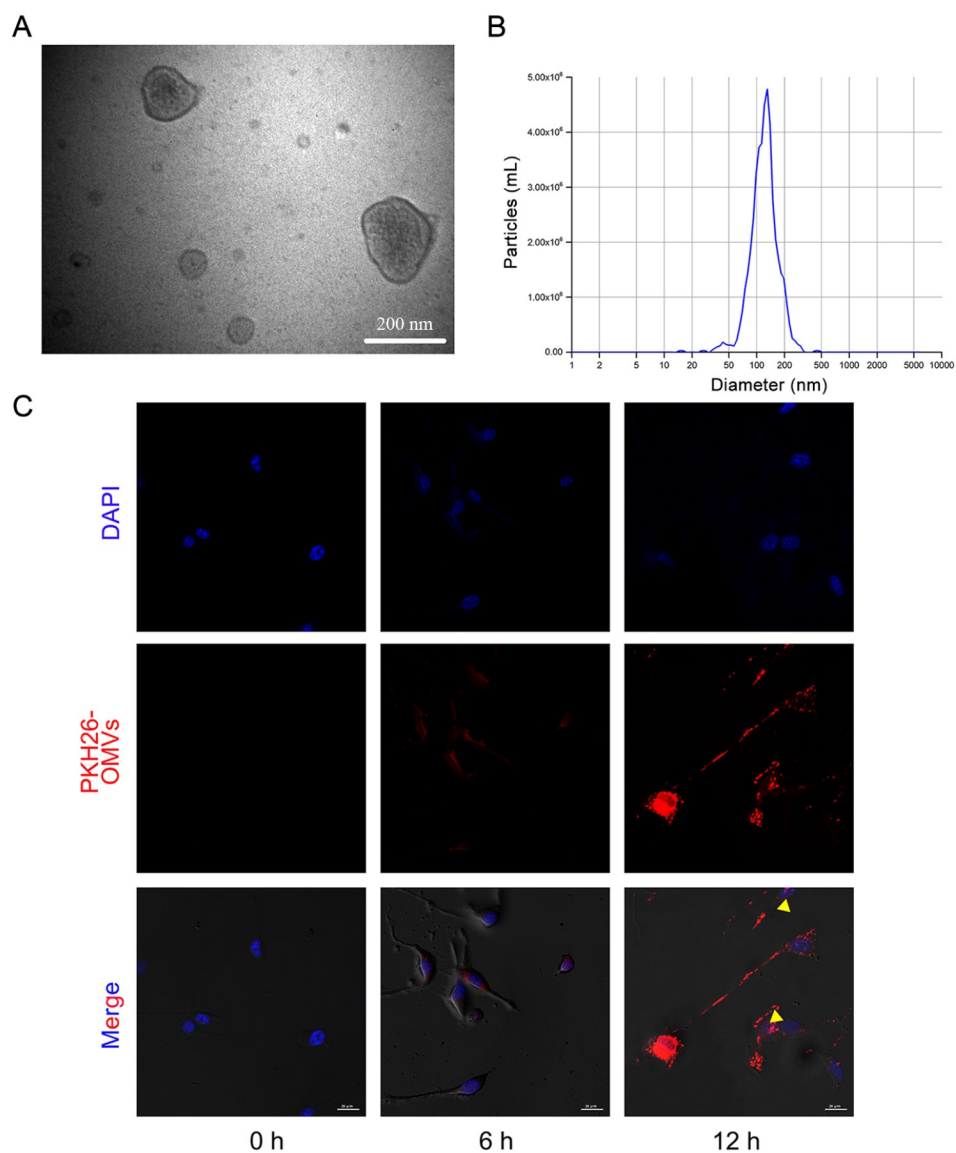


Figure 1. Identification of *E. coli*-OMVs and internalization of *E. coli*-OMVs (A) Spherical structure of *E. coli*-OMVs as observed by TEM. Scale bar: 200 nm. (B) NTA measurement of size and concentration distribution revealed a mean particle diameter of 119.5 ± 2.95 nm and concentration of 1.83 × 10⁸ particles/µL, *n* = 3. (C) Internalization of *E. coli*-OMVs into SK-N-SH cells. Red fluorescence indicates PKH26-labelled *E. coli*-OMVs, and △ indicates *E. coli*-OMVs in the nucleus. Scale bar: 20 µm.

1 µg/µL suspension according to the BCA assay. We used a bacterial Lipopolysaccharide (LPS) ELISA kit to quantify the LPS level in the extracted *E. coli*-OMVs, and the results suggested that the 1 mg/mL *E. coli*-OMV suspension contained 0.07 EU/mL of endotoxin LPS. Confocal microscopy showed that cells treated with PKH26-labelled *E. coli*-OMVs presented notable red fluorescence in the cytoplasm and nucleus, and tumor cells exhibited some specific morphological changes, such as chromatin condensation. Red fluorescence was first observed at 6 h; then, the intensity became stronger at 12 h (Figure 1C).

Cytotoxicity of *E. coli*-OMVs *in vitro*

E. coli-OMVs exhibited dose-dependent cytotoxicity (Figure 2A); the IC₅₀ value of *E. coli*-OMVs for SK-N-SH cells was 177.5 µg/mL (3.15×10^{10} particles/mL), the IC₅₀ value for SH-SY5Y cells was 149.5 µg/mL (2.74×10^{10} particles/mL), and the IC₅₀ value for HEK293 cells was 251.8 µg/mL (4.61×10^{10} particles/mL). The cytotoxicity of *E. coli*-OMVs at the IC₅₀ concentration for SK-N-SH cells exerted a stable suppressive effect on cell proliferation, which was verified at 24, 48, and 72 h (Figure 2A). Therefore, the dose of 177.5 µg/mL (3.15×10^{10} particles/mL) *E. coli*-OMVs used to treat SK-N-SH cells in all the *in vitro* experiments in this study.

The protein expression of PCNA in cells was measured after treatment with *E. coli*-OMVs for 48 h, and this expression was significantly suppressed compared to that observed in the control. To explore whether the attenuated proliferation capacity is related to changes in cell pluripotency, the expressions of the following proteins were measured: N-myc, SOX-2, OCT-4 and NANOG. Similar to the trend of PCNA expression, the expressions of these proteins were obviously decreased after treatment with *E. coli*-OMVs (Figure 2B).

The cell cycle distribution results showed an increase in the percentage of cells in the S phase and significant decreases in the percentages of cells in the G0/G1 and G2/M phases after treatment with *E. coli*-OMVs. Moreover, there was a distinct increase in the number of apoptotic cells in the *E. coli*-OMV-treated group (Figure 2C). Accordingly, western blot analysis results indicated that the protein expressions of cyclin A and CDK2 in the intervention group were decreased, while the protein expression of P21 was increased (Figure 2D). The change in the expressions of proteins related to the S phase was consistent with the results of the cell cycle assay, confirming that the cells were arrested in the S phase.

Proapoptotic effect of *E. coli*-OMVs

Annexin V was used to quantitatively measure the number of apoptotic cells, and the results revealed distinct increases in the number of apoptotic cells in both NB-cell lines. Among the *E. coli*-OMV-treated cells, apoptosis occurred in 18.85% of SK-N-SH cells and in 35.42% of SH-SY5Y cells, while only 7.81% of HEK293 cells underwent apoptosis. (Figure 3A). The TUNEL assay revealed obvious chromosomal breaks in the *E. coli*-OMV-treated cells, which indicated that the cells were induced to undergo apoptosis (Figure 3B). Since apoptosis and DNA damage were observed after treatment with *E. coli*-OMVs, the protein expression of p53 was examined; however, no change was observed between the *E. coli*-OMV-treated and control groups. Therefore, we measured the level of phosphorylated P53 (phospho-P53), which was significantly increased after treatment with *E. coli*-OMVs (Figure 3C). Moreover, the mitochondrial apoptosis pathway was activated in the *E. coli*-

OMV-treated cells, and the expressions of proteins related to mitochondrial apoptosis were changed significantly. The expression of the antiapoptotic protein BCL-2 was downregulated, and the expression of the proapoptotic protein BAX was upregulated. Cyt c, a mitochondrial respiratory chain electron transfer-associated protein, was detected at significantly high level in the cytoplasm of *E. coli*-OMV-treated cells, while Cyt c protein expression was extremely low in the cytoplasm of control cells. Compared to that of the control group, Cyt c protein expression was significantly reduced among the mitochondrial proteins of the *E. coli*-OMV-treated group (Figure 3D). The expression of the downstream protein Apaf was increased as expected. Finally, cleaved caspase-3, a typical hallmark of apoptosis, was activated, indicating the occurrence of apoptosis (Figure 3D).

The inhibitory effect of *E. coli*-OMVs on cell migration and invasion

In the wound healing assay, the scratch area of the treated groups was larger than that of the control groups at 24 h and 48 h (Figure 4A), which indicated that the migration of cells was decreased by *E. coli*-OMVs. In addition, the Transwell invasion assay revealed that the number of cells that penetrated through the Matrigel was significantly lower in the *E. coli*-OMV group than in the control group (Figure 4B). The western blot analysis results showed that the expressions of MMP-2, MMP-9, VEGF, and CD24 were obviously decreased in the *E. coli*-OMV-treated group compared to those in the control group (Figure 4C).

Antineoplastic activity of *E. coli*-OMVs *in vivo*

We tested whether *E. coli*-OMVs cause a significant acute systemic inflammatory response in BALB/c mice. The mice in the normal group and *E. coli*-OMV group were active, with white, fine and lustrous fur, shiny eyes, and brown-black and well-formed stools. At 24 h after injection, the mice in the LPS group were curled up and less active, with wet, sticky and less lustrous fur, slightly closed eyes, and unformed stools. The anal temperature, white blood cell (WBC) count and classification, and blood glucose levels of the mice in the three groups are shown in Table 1.

There was no significant difference in body temperature between the mice in all groups before injection, and 24 h after injection, there was no significant difference between the *E. coli*-OMV group and the control group; the rectal temperature of the mice in the LPS group was significantly lower than that of the mice in the control group ($P < 0.01$). The WBC count, neutrophil ratio and blood glucose level in the *E. coli*-OMV group were not significantly different from those in the control group, while the mice in the LPS group showed a significant decrease in the WBC count, an increase in the neutrophil ratio and a decrease in the blood glucose level.

We injected DIR-fluorescently labelled *E. coli*-OMVs into BALB/c mice with SK-N-SH tumors via the tail vein and performed *in vivo* imaging experiments at 24 h and 48 h postinjection. We found that *E. coli*-OMVs were delivered to the tumor site 24 h after injection. At 24 h, the sites to which the *E. coli*-OMVs were distributed in the highest amounts *in vivo* were the liver, tumor, lung and spleen. At 48 h, fluorescence still significantly accumulated in the liver and tumor, and basically disappeared from other sites (Figure 5A).

In BALB/c nude mice, after intravenous injection with *E. coli*-OMVs, the total body weights of the mice showed no significant difference among the five groups (Figure 5B). Daily monitoring of

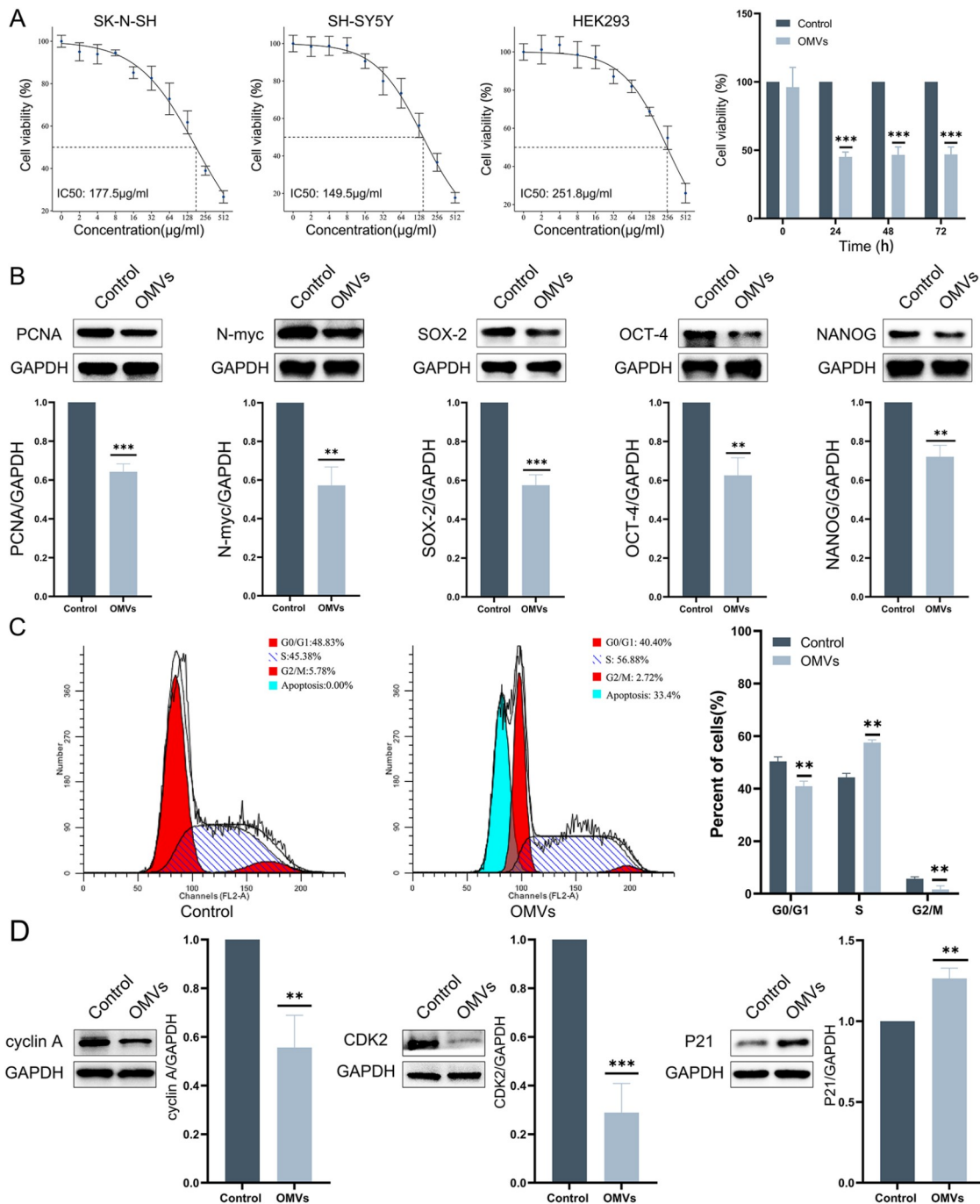


Figure 2. *E. coli*-OMVs induce cell proliferation inhibition and cell cycle arrest (A) The viabilities of SK-N-SH, SH-SY5Y and HEK293 cells were measured by CCK-8 assay after treatment with *E. coli*-OMVs (0, 2, 4, 8, 16, 32, 64, 128, 256 and 512 µg/mL) for 48 h. (B) Western blot analysis of PCNA, N-myc, SOX-2, OCT-4, and NANOG expressions. (C) Cell cycle analysis. (D) Western blot analysis of cyclin A, CDK2, and p21 expressions. Data are presented as the mean \pm SD, $n=3$. * $P<0.05$, ** $P<0.01$, and *** $P<0.001$ vs the control group. ns, no significant difference.

the tumor size revealed that the tumors in the treatment groups grew significantly slower than those in the control groups, and this reduction was dose-dependent within a certain range. Ultimately, the average tumor volume in the high-dose group was less than half of that in the control groups. The tumors were collected at the end point, and the average weights of the tumors in the three treatment groups were lower than those in the control group (Figure 5C,D). The results of HE staining of tumors showed obvious tissue damage,

such as hemorrhage and necrosis, in the tumors of the treatment groups (Figure 6A). We also examined the damages to the liver, kidney, heart and lung tissues, and no significant difference was observed in the *E. coli*-OMV groups (Figure 6B). We analysed the serum from the nude mice and measured the serum levels of ALT, AST, AST/ALT, Cr and BUN, which are key indicators of liver and kidney injury. No statistically significant differences were observed between the treatment groups and control groups (Figure 6C). In

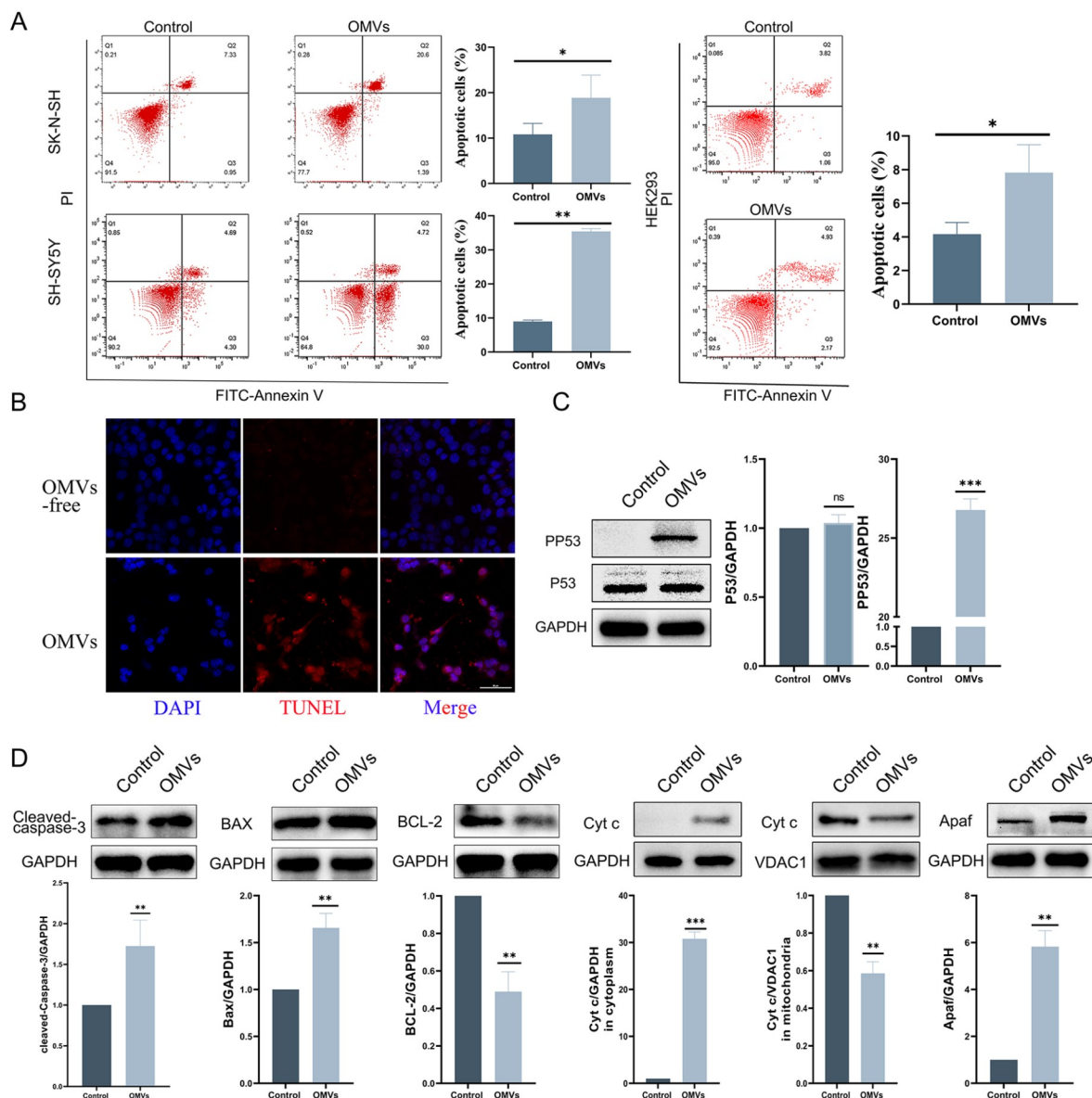


Figure 3. *E. coli*-OMVs induce apoptosis of SK-N-SH, SH-SY5Y and HEK293 cells (A) Apoptosis of cells measured by Annexin V. (B) TUNEL assay. Scale bar: 50 μ m. (C) Western blot analysis of P53 and phospho-P53 expressions. (D) Western blot analysis of cleaved caspase-3, BAX, BCL-2, Cyt c and Apaf expressions. Data are presented as the mean \pm SD, $n=3$. * $P<0.05$, ** $P<0.01$, and *** $P<0.001$ vs the control group. ns, no significant difference.

addition, a liver with obvious nodules was observed in one of the mice in the control group. We recorded a general picture and performed a pathological examination of the tissue (Supplementary Figure S1).

Antitumor activity of *E. coli*-OMVs

Immunohistochemical staining of the expressions of the proliferation marker (PCNA), invasion marker (MMP-9) and angiogenic activity marker (VEGF) in tumor tissues were performed to investigate the antitumor activity of *E. coli*-OMVs. The results showed very weak staining for all three markers in tumors of the treatment groups compared with those in tumors of the control groups (Figure 7A). Additionally, the protein expressions of PCNA,

MMP-9 and VEGF were measured by western blot analysis, and the results showed significant decreases in the *E. coli*-OMV groups (Figure 7B). The above results indicated that OMV intervention reduced the growth, invasiveness and angiogenic activity of tumor tissues. Moreover, the TUNEL assay indicated that tumors treated with *E. coli*-OMVs displayed a higher fluorescence intensity of dTTP, which indicated that apoptosis occurred at higher rates in tumors from the treatment groups than in those from the control groups (Figure 7C).

Discussion

The use of bacteria as antitumor drugs has been discussed since the last century, but this treatment has some drawbacks, namely, a high

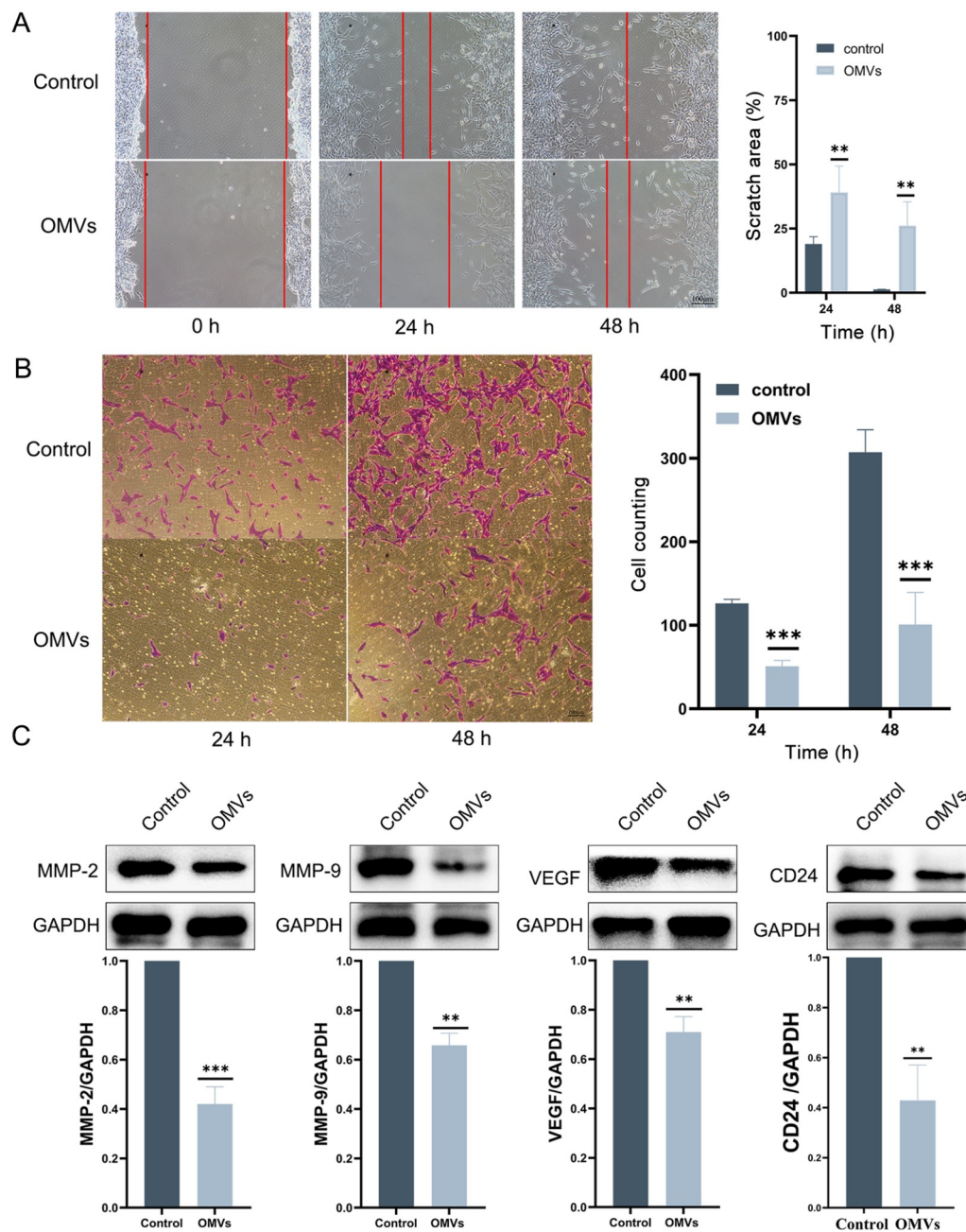


Figure 4. *E. coli*-OMVs inhibit the migration of SK-N-SH cells (A) Migration of cells measured by wound healing assay. Scale bar: 100 μ m. (B) Invasion of cells measured by Transwell assay. Scale bar: 100 μ m. (C) Western blot analysis of MMP-2, MMP-9 VEGF and CD24 expressions. Data are presented as the mean \pm SD, $n=3$. * $P<0.05$, ** $P<0.01$, and *** $P<0.001$ vs the control group. ns, no significant difference.

Table 1. Inflammatory response in BALB/c mice

Group	n	Rectal temperature ($^{\circ}$ C)		WBCs ($\times 10^9$ cells/L)	Neutrophils (%)	Glucose (mM)
		Before	After			
Control	5	36.0 \pm 0.27	35.8 \pm 0.14	5.82 \pm 0.61	4.8 \pm 1.33	9.4 \pm 2.68
OMVs	5	35.7 \pm 0.22 ^{ns}	35.7 \pm 0.32 ^{ns}	5.67 \pm 0.9 ^{ns}	4 \pm 0.67 ^{ns}	9.1 \pm 2.6 ^{ns}
LPS	5	36.1 \pm 0.38 ^{ns}	32.5 \pm 0.32 ^{**}	4.21 \pm 0.78 [*]	24.0 \pm 6.98 ^{**}	3.3 \pm 0.74 ^{**}

* $P<0.05$, ** $P<0.01$ compared with the control group. ns, not significant.

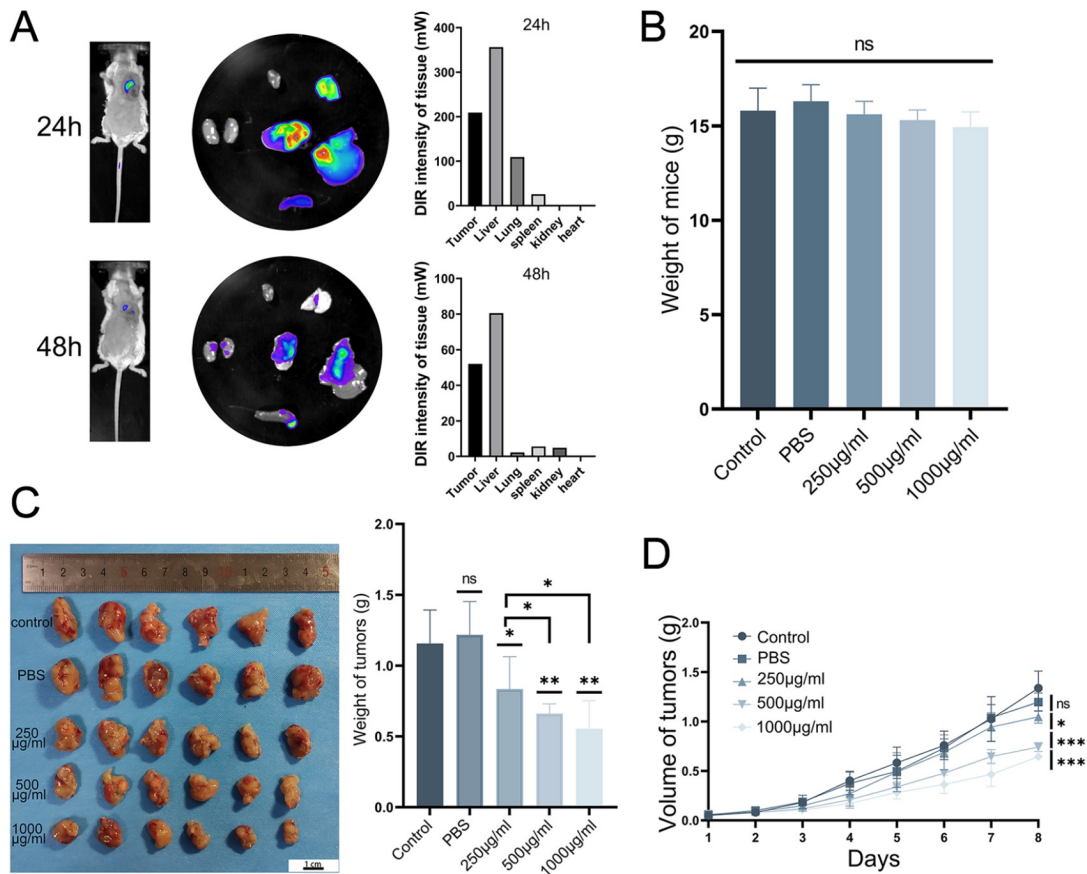


Figure 5. *In vivo* distribution and antitumor effects of *E. coli*-OMVs (A) *In vivo* distribution of *E. coli*-OMVs. (B) Weight of tumor-bearing mice. (C) Anatomical image of tumors and weight of tumors. Scale bar: 1 cm. (D) Tumor volume. Data are presented as the mean \pm SD, $n=6$. * $P<0.05$, ** $P<0.01$, and *** $P<0.001$ vs the control group. ns, no significant difference.

risk of systemic bacterial infection and increased toxicity [15-17]. Bacterial OMVs have been found to have advantages in adjuvant immunotherapy and targeted drug delivery [18]. Initially, De [19] identified a vesicular substance from *Vibrio cholerae*; subsequently, Knox *et al.* [20] discovered a vesicular material with a lipid bilayer structure of approximately 20–500 nm in diameter that is secreted by *E. coli*; this material was defined as extracellular vesicles. Upon binding to a target cell, the bioactive substances within these vesicles can be transported into the host cell, thereby altering its biological activity.

In this study, *E. coli* was selected for the extraction of OMVs. The academically accepted methods of OMV identification involve TEM to observe their morphology and NTA to measure their diameter. The extracted components were found to have a circular membrane vesicle structure, contain material of variable density, and have a diameter distribution from 45 to 285 nm, which are consistent with the definition of bacterial OMVs, indicating that we successfully extracted *E. coli*-OMVs. Then, we examined the levels of endotoxin LPS contained in these *E. coli*-OMVs.

OMVs can be taken up by tumor cells and exert biological functions. Previously, it was found that tumor cells can phagocytose OMVs into the cytosol after 2 to 4 h [21,22]. In this study, *E. coli*-OMVs were found to be taken up by SK-N-SH cells after 6 h, and intracellular OMVs became more abundant at 12 h. In addition,

some OMVs were observed to enter the nucleus. Bielaszewska *et al.* [23] reported that *E. coli*-OMVs, after being internalized into cells, can be intracellularly transported via processes that are dependent on intracytoplasmic solute transfer complexes and the endoplasmic reticulum and can eventually reach the nucleus and cause DNA damage. Our study verified that *E. coli*-OMVs can be internalized, translocate within the cell and further localize to the nucleus.

We examined the cytotoxicity of *E. coli*-OMVs on SK-N-SH cells, and *E. coli*-OMVs at the IC_{50} concentration was used in all the subsequent *in vitro* experiments. We found that *E. coli*-OMVs inhibited the proliferative activity of cells. It is believed that some cells in cancers have the ability to self-renew and produce heterogeneous tumor cells; which are known as cancer stem cells, and they have been shown to play an important role in tumor survival, proliferation, metastasis, and recurrence [24]. Therefore, we measured the expressions of multiple proteins associated with cell pluripotency, including SOX2, OCT4 and NANOG [25-27], and the expressions of all of these proteins were significantly decreased. Some studies have reported that the N-myc protein is associated with the activation of stem cell-like properties of cells [28,29]. The expression of this protein was also decreased after treatment with *E. coli*-OMVs. N-myc is a member of the MYC family of transcription factors, and enhanced or dysregulated expression of N-myc promotes the development of a variety of tumors [30]. Over-

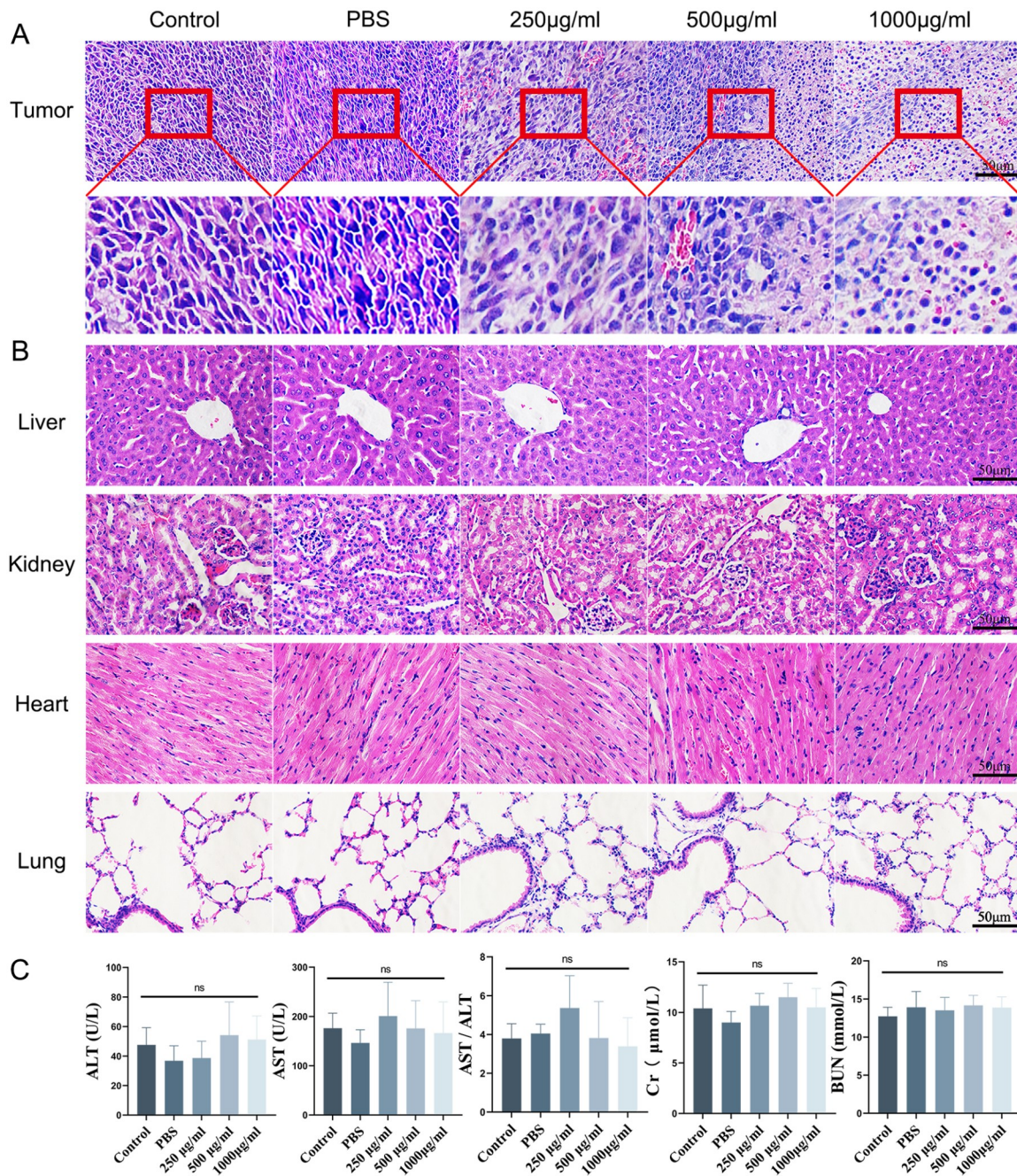


Figure 6. HE staining of tissues, and changes in liver and kidney function (A) HE-stained tumor tissue. Scale bar: 50 µm. (B) HE-stained liver, kidney, heart, and lung tissues of mice after treatment. Scale bar: 50 µm. (C) Liver and kidney function of mice.

expression of the N-myc protein in NB is the initiating factor that drives the development of high-risk NB and is usually associated with poor prognosis [31]. Although SK-N-SH cells are a non-MYC-amplified NB-cell line, we still found a significant decrease in N-myc protein expression in the treated cells. This led us to wonder whether *E. coli*-OMVs can be used to suppress high-risk NB with MYCN gene amplification. Overall, the decrease in cell stemness could lead to the inhibition of cell proliferation.

Significant DNA damage and apoptosis were observed in treated cells. DNA damage causes P53 activation; the latter can activate the former, which can lead to cell cycle arrest and apoptosis [32]. We

measured P53 expression; however, its expression was not significantly altered. Considering that P53 exists in a dynamic balance between continuous translation and constant degradation in cells, we focused on its posttranscriptional modifications. We measured the levels of phospho-P53 and observed a significant increase of phospho-P53 in treated cells. It has been well established that phospho-P53 can regulate apoptosis by activating the BCL-2 family of proapoptotic genes [33]. We observed a significant decrease in the expression of the suppressor protein BCL-2 and a significant increase in the expression of the proapoptotic protein BAX. The key protein Cyt c was activated, followed by Apaf protein

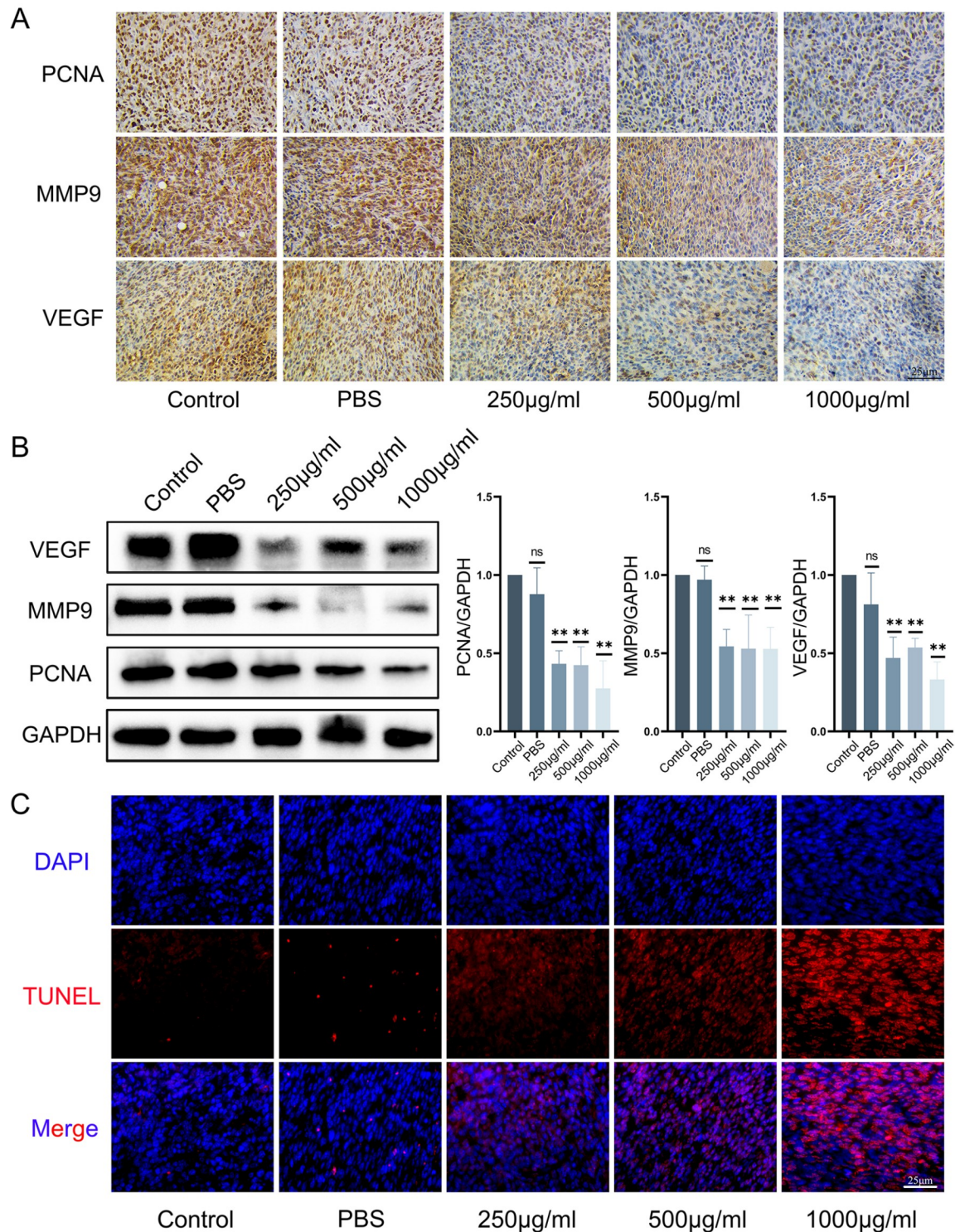


Figure 7. Immunohistochemistry, immunofluorescence and western blot analysis of tumor tissues (A) Immunohistochemical images of PCNA, MMP-9 and VEGF expressions. Scale bar: 25 µm. (B) Western blot analysis of PCNA, MMP-9 and VEGF expressions. (C) TUNEL assay. Scale bar: 25 µm. Data are presented as the mean \pm SD, $n=3$. * $P<0.05$, ** $P<0.01$, and *** $P<0.001$ vs the control group. ns, no significant difference.

in the cytoplasm. Theoretically, the combination of activated Cyt c and Apaf could reactivate the downstream caspase-3 to eventually cause apoptosis, and our results showed that the expression of activated cleaved caspase-3 was significantly increased. The above

changes indicate that the mitochondrial apoptotic pathway is activated. Therefore, we conclude that treatment with *E. coli*-OMVs induces DNA damage and mitochondria-mediated apoptosis in tumor cells.

In addition, P53 is an important regulator of the cell cycle and proliferation. Excessive levels of phospho-P53 can activate the P21 protein and inhibit the PCNA protein, leading to cell cycle arrest and inhibition of cell proliferation [34,35]. In this study, *E. coli*-OMVs resulted in significant S-phase arrest, suggesting a possible impairment of cellular DNA replication. The cyclin A/CDK2 complex acts as a regulator of the S phase [36], and downregulation of the expression of cyclin A and CDK2 was observed, while that of the P21 protein (a repressor of the cyclin A/CDK2 complex) was significantly upregulated [37,38]. Thus, *E. coli*-OMVs may affect DNA replication, resulting in cell cycle failure. The protein expression of PCNA was significantly inhibited in the treated groups *in vitro* and *in vivo*. When cells experience DNA damage, the PCNA protein plays an important stabilizing role in cellular DNA replication and serves as a scaffolding protein for organizing DNA repair and providing bypass pathways. Furthermore, PCNA has been shown to be involved in the regulation of cell cycle proteins (such as p53 and P21) to maintain the cell cycle [39,40]. Thus, dysfunction of PCNA could mitigate cell proliferation.

Combining the above results, we infer that treatment with *E. coli*-OMVs reduces the proliferative activity of tumor cells, most likely due to the following three reasons: first, the pluripotent potential of treated tumor cells is inhibited, and their self-renewal ability is diminished; second, some of the viable cells show signs of apoptosis, resulting in a decrease in overall cell activity; and third, treated cells are unable to successfully complete the cell cycle due to the occurrence of DNA damage, failure of the Cyclin A/CDK2 complex and inhibition of PCNA.

This study showed that treatment of SK-N-SH cells with *E. coli*-OMVs inhibited the migratory and invasive abilities of these cells. CD24 expression is specifically increased in a variety of cancers and is associated with the malignant proliferation and invasion of tumors. The expression level of CD24 is elevated in NB, and CD24 expression is associated with NB invasion and poor prognosis [41]. Our study indicated that cells treated with *E. coli*-OMVs showed significant downregulation of CD24, MMP-2, and MMP-9 protein expressions; these proteins are closely associated with tumor invasion and metastasis [42]. In addition, tumor growth and invasion are closely related to tumor neovascular formation, and VEGF expression is downregulated [43]. Suppression of MMP-9 and VEGF expression was observed in tumors of the three treatment groups, which suggests that *E. coli*-OMVs can still inhibit tumor invasive capacity and angiogenic activity *in vivo*. We conclude that *E. coli*-OMVs can inhibit the malignant metastasis and invasive abilities of NB. Refractory NB often has the malignant manifestations of early distant metastasis and recurrent metastasis after treatment, and new therapeutic ideas are required for the early prevention of NB distant metastasis. However, although we observed that the invasive ability of tumor tissues was inhibited, we only observed liver metastasis in the control groups, which was not enough to support our point. This may be attributed to the termination of the treatment experiment when the tumor volume reached a certain size based on animal ethical considerations, and this termination may have occurred before the tumor reached the metastasis stage. Therefore, we think that the inhibitory effect of *E. coli*-OMVs on invasive metastasis may need to be demonstrated in additional follow-up studies, and this study can provide support for these future studies.

We further verified the inhibitory effect of *E. coli*-OMVs on NB *in*

vivo in a subcutaneous heterograft tumor model established in nude mice. The size of the monitored subcutaneous masses, the tumors observed at biopsy, and the excised tumor tissue provided encouraging results: all three doses of *E. coli*-OMVs exerted an inhibitory effect on the growth of the tumors, and this effect was dose dependent. However, compared to previous findings by Kim *et al.* [10], we did not observe complete clearance of NB, which may be due to the differences in the experimental protocol: we used immunodeficient nude mice as a model, and *E. coli*-OMVs may be more effective against intestinal tumors. We observed a trend of weight loss in the nude mice, but the difference was not statistically significant. Additionally, we performed HE staining of several vital organs, including the heart, liver, lung, and kidney, to observe their morphologies. We did not observe significant differences between the groups. We demonstrated that the effective doses we used did not cause acute systemic inflammatory reactions and did not significantly impair liver or kidney function in mice. These findings at least indicate that the starting dose we used did not cause serious side effects.

In conclusion, we present the use of *E. coli*-OMVs as an adjuvant therapy for NB without significant adverse effects. Our mechanistic studies suggest that these nanosized vesicles can enter the cell cytoplasm and nucleus, and decrease cell stemness, DNA damage, apoptosis and cell cycle arrest to exert a combined antitumor effect. An approach to cancer treatment based on bacterial OMVs may provide new directions in future research.

Funding

This work was supported by the grant from the Special Project of Technology Innovation and Application Development of Chongqing (No. cstc2019jcsx-tjsbX0003).

Conflict of Interest

The authors declare that they have no conflict of interest.

References

1. Siegel RL, Miller KD, Fuchs HE, Jemal A. Cancer statistics, 2021. *CA Cancer J Clin* 2021, 71: 7–33
2. Helmink BA, Khan MAW, Hermann A, Gopalakrishnan V, Wargo JA. The microbiome, cancer, and cancer therapy. *Nat Med* 2019, 25: 377–388
3. Sivan A, Corrales L, Hubert N, Williams JB, Aquino-Michaels K, Earley ZM, Benyamin FW, *et al.* Commensal *Bifidobacterium* promotes anti-tumor immunity and facilitates anti-PD-L1 efficacy. *Science* 2015, 350: 1084–1089
4. Vétizou M, Pitt JM, Daillère R, Lepage P, Waldschmitt N, Flament C, Rusakiewicz S, *et al.* Anticancer immunotherapy by CTLA-4 blockade relies on the gut microbiota. *Science* 2015, 350: 1079–1084
5. Chen Q, Huang G, Wu W, Wang J, Hu J, Mao J, Chu PK, *et al.* A hybrid eukaryotic-prokaryotic nanoplatform with photothermal modality for enhanced antitumor vaccination. *Adv Mater* 2020, 32: 1908185
6. Qing S, Lyu C, Zhu L, Pan C, Wang S, Li F, Wang J, *et al.* Biomimetic bacterial outer membrane vesicles potentiate safe and efficient tumor microenvironment reprogramming for anticancer therapy. *Adv Mater* 2020, 32: 2002085
7. Toyofuku M, Nomura N, Eberl L. Types and origins of bacterial membrane vesicles. *Nat Rev Microbiol* 2019, 17: 13–24
8. Chen Q, Bai H, Wu W, Huang G, Li Y, Wu M, Tang G, *et al.* Bioengineering bacterial vesicle-coated polymeric nanomedicine for enhanced cancer immunotherapy and metastasis prevention. *Nano Lett* 2020, 20: 11–21

9. Gujrati V, Kim S, Kim SH, Min JJ, Choy HE, Kim SC, Jon S. Bioengineered bacterial outer membrane vesicles as cell-specific drug-delivery vehicles for cancer therapy. *ACS Nano* 2014, 8: 1525–1537
10. Kim OY, Park HT, Dinh NTH, Choi SJ, Lee J, Kim JH, Lee SW, *et al.* Bacterial outer membrane vesicles suppress tumor by interferon- γ -mediated antitumor response. *Nat Commun* 2017, 8: 626
11. Aly RG, El-Enbaawy MI, Abd El-Rahman SS, Ata NS. Antineoplastic activity of Salmonella Typhimurium outer membrane nanovesicles. *Exp Cell Res* 2021, 399: 112423
12. Matthay KK, Maris JM, Schleiermacher G, Nakagawara A, Mackall CL, Diller L, Weiss WA. Neuroblastoma. *Nat Rev Dis Primers* 2016, 2: 16078
13. Shohet J, Foster J. Neuroblastoma. *BMJ* 2017, 357: j1863
14. Zhu S, Zhang X, Weichert-Leahey N, Dong Z, Zhang C, Lopez G, Tao T, *et al.* LMO1 synergizes with MYCN to promote neuroblastoma initiation and metastasis. *Cancer Cell* 2017, 32: 310–323.e5
15. Toso JF, Gill VJ, Hwu P, Marincola FM, Restifo NP, Schwartzentruber DJ, Sherry RM, *et al.* Phase I study of the intravenous administration of attenuated *salmonella typhimurium* to patients with metastatic melanoma. *J Clin Oncol* 2002, 20: 142–152
16. Zhou S, Gravekamp C, Bermudes D, Liu K. Tumour-targeting bacteria engineered to fight cancer. *Nat Rev Cancer* 2018, 18: 727–743
17. Galloway-Peña J, Brumlow C, Shelburne S. Impact of the microbiota on bacterial infections during cancer treatment. *Trends Microbiol* 2017, 25: 992–1004
18. Sui X, Liang X, Chen L, Guo C, Han W, Pan H, Li X. Bacterial xenophagy and its possible role in cancer: A potential antimicrobial strategy for cancer prevention and treatment. *Autophagy* 2017, 13: 237–247
19. De SN. Enterotoxicity of bacteria-free culture-filtrate of *Vibrio cholerae*. *Nature* 1959, 183: 1533–1534
20. Knox KW, Vesk M, Work E. Relation between excreted lipopolysaccharide complexes and surface structures of a lysine-limited culture of *Escherichia coli*. *J Bacteriol* 1966, 92: 1206–1217
21. Li Y, Zhao R, Cheng K, Zhang K, Wang Y, Zhang Y, Li Y, *et al.* Bacterial outer membrane vesicles presenting programmed death 1 for improved cancer immunotherapy via immune activation and checkpoint inhibition. *ACS Nano* 2020, 14: 16698–16711
22. Cheng K, Zhao R, Li Y, Qi Y, Wang Y, Zhang Y, Qin H, *et al.* Bioengineered bacteria-derived outer membrane vesicles as a versatile antigen display platform for tumor vaccination via Plug-and-Display technology. *Nat Commun* 2021, 12: 2041
23. Bielaszewska M, Rüter C, Bauwens A, Greune L, Jarosch KA, Steil D, Zhang W, *et al.* Host cell interactions of outer membrane vesicle-associated virulence factors of enterohemorrhagic *Escherichia coli* O157: intracellular delivery, trafficking and mechanisms of cell injury. *PLoS Pathog* 2017, 13: e1006159
24. Lytle NK, Barber AG, Reya T. Stem cell fate in cancer growth, progression and therapy resistance. *Nat Rev Cancer* 2018, 18: 669–680
25. Jeter CR, Yang T, Wang J, Chao HP, Tang DG. Concise review: NANOG in cancer stem cells and tumor development: an update and outstanding questions. *Stem Cells* 2015, 33: 2381–2390
26. Novak D, Hüser L, Elton JJ, Umansky V, Altevogt P, Utikal J. SOX2 in development and cancer biology. *Semin Cancer Biol* 2020, 67: 74–82
27. Villodre ES, Kipper FC, Pereira MB, Lenz G. Roles of OCT4 in tumorigenesis, cancer therapy resistance and prognosis. *Cancer Treatment Rev* 2016, 51: 1–9
28. King B, Boccalatte F, Moran-Crusio K, Wolf E, Wang J, Kayembe C, Lazaris C, *et al.* The ubiquitin ligase Huwe1 regulates the maintenance and lymphoid commitment of hematopoietic stem cells. *Nat Immunol* 2016, 17: 1312–1321
29. Molenaar JJ, Domingo-Fernández R, Ebus ME, Lindner S, Koster J, Drabek K, Mestdagh P, *et al.* LIN28B induces neuroblastoma and enhances MYCN levels via let-7 suppression. *Nat Genet* 2012, 44: 1199–1206
30. Rickman DS, Schulte JH, Eilers M. The expanding world of N-MYC-Driven tumors. *Cancer Discovery* 2018, 8: 150–163
31. Lee JK, Phillips JW, Smith BA, Park JW, Stoyanova T, McCaffrey EF, Baertsch R, *et al.* N-Myc drives neuroendocrine prostate cancer initiated from human prostate epithelial cells. *Cancer Cell* 2016, 29: 536–547
32. Kasthuber ER, Lowe SW. Putting p53 in context. *Cell* 2017, 170: 1062–1078
33. Chandrasekar AP, Cummins NW, Badley AD. The Role of the BCL-2 Family of Proteins in HIV-1 Pathogenesis and Persistence. *Clin Microbiol Rev* 2019, 33: e00107
34. Hong H, Takahashi K, Ichisaka T, Aoi T, Kanagawa O, Nakagawa M, Okita K, *et al.* Suppression of induced pluripotent stem cell generation by the p53–p21 pathway. *Nature* 2009, 460: 1132–1135
35. Seoane J, Le HV, Massagué J. Myc suppression of the p21Cip1 Cdk inhibitor influences the outcome of the p53 response to DNA damage. *Nature* 2002, 419: 729–734
36. Kamer I, Sarig R, Zaltsman Y, Niv H, Oberkovitz G, Regev L, Haimovich G, *et al.* Proapoptotic BID is an ATM effector in the DNA-damage response. *Cell* 2005, 122: 593–603
37. Maya-Mendoza A, Moudry P, Merchut-Maya JM, Lee MH, Strauss R, Bartek J. High speed of fork progression induces DNA replication stress and genomic instability. *Nature* 2018, 559: 279–284
38. Deng C, Zhang P, Wade Harper J, Elledge SJ, Leder P. Mice lacking p21CIP1/WAF1 undergo normal development, but are defective in G1 checkpoint control. *Cell* 1995, 82: 675–684
39. Mailand N, Gibbs-Seymour I, Bekker-Jensen S. Regulation of PCNA-protein interactions for genome stability. *Nat Rev Mol Cell Biol* 2013, 14: 269–282
40. González-Magaña A, Blanco FJ. Human PCNA structure, function and interactions. *Biomolecules* 2020, 10: 570
41. Altevogt P, Sammar M, Hüser L, Kristiansen G. Novel insights into the function of CD24: A driving force in cancer. *Int J Cancer* 2021, 148: 546–559
42. Jacob A, Prekeris R. The regulation of MMP targeting to invadopodia during cancer metastasis. *Front Cell Dev Biol* 2015, 3: 4
43. Apte RS, Chen DS, Ferrara N. VEGF in signaling and disease: beyond discovery and development. *Cell* 2019, 176: 1248–1264